Fast Radio Bursts and their possible origin as collisions between stars and cold dark matter in the form of primordial black holes

Moskvitch, Ekaterina

Awarding institution:
King's College London

Prepared for submission to MPhil

Fast Radio Bursts and their possible origin as collisions between stars and cold dark matter in the form of primordial black holes

Ekaterina Moskvitch

MPhil Thesis, King's College London. Primary supervisor: Prof. Malcolm Fairbairn

Abstract. Fast Radio Bursts (FRBs) are ultra-brief, ultra-powerful bursts of energy of unknown source that seem to be originating in distant galaxies. Here, we propose that they could be produced when primordial black holes, a cold dark matter candidate, collide with stars, via the phenomenon of superradiance occurring in the plasma of the transition region of stars. We calculate the number of such collisions per year, and compare it to the estimates of the rates of FRB events in the Universe. We find that, even with the most generous assumptions, the rate of FRBs cannot be fully accounted for by this source alone. Thus, whilst this is a plausible source of FRBs, it cannot be the only one.

Contents

1 INTRODUCTION

Fast Radio Bursts (FRBs) are some of the brightest flashes in the universe. These ultra-brief, some in the range of 1-10 ms and some $\lesssim$1 ms long, superenergetic transient signals observed at radio frequencies of (at the time of writing) $f \sim 1$ GHz [1]. Based on the measured dispersion measure exceeding the Galactic value, they seem to be of extragalactic origin. Currently, 75 FRBs have been published in the FRB catalogue (see the online catalogue on http://frbcat.org), and $\sim$ dozens more have been detected but not yet published. In January, the Canadian Hydrogen Intensity Mapping Experiment (CHIME) published in Nature the detection of 13 new bursts, among them one repeater (the second repeater ever detected) [2]. 18 FRBs are shown on Fig. 2. The observed energy of FRBs is $\sim 10^{32} - 10^{33}$ J across the burst, with luminosities of $\sim 10^{41} - 10^{42}$erg/s [1] [3] [4].

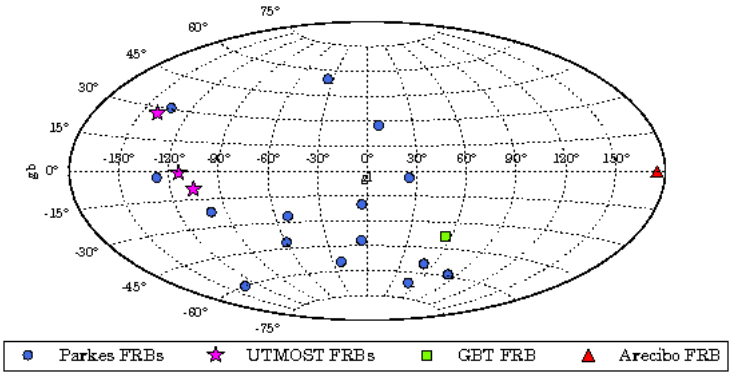

Figure 1: The sky distribution of the 18 FRBs. Dots mark the positions of the FRBs detected at the Parkes telescope, the triangle represents FRB 121102 detected at the Arecibo telescope and the square represents FRB 110523 discovered at the Green Bank Telescope. Figure from Caleb et al. (2017)[5].

Their nature is unknown. It remains a mystery whether all FRB sources represent a single population, as well as their exact distance scale and typical luminosity. Determining the origin could help to better understand the nature of their host galaxies. In cosmology, pinpointing FRBs at different cosmological distances could help measure the amount of matter spread out in space between the Earth and their sources. Such measurements are important to confirm simulations that suggest the Universe shows a particular 'clumpy' structure, with clusters and voids - and also could shed more light on the distribution of dark matter. In the near future, new technology and next-generation radio telescopes, such as the Square Kilometer Array in South Africa and Australia [6] and the newly-built Canadian Hydrogen Intensity Mapping Experiment (CHIME) [7], will be crucial in the search for the origins of the bursts.

The first FRB (FRB010724), Fig. 2, was reported in 2007 by Lorimer [1], found in the archival 2001 data from a pulsar survey of the Magellanic Clouds of the 64m Parkes Radio Telescope in Australia. It was characterised by its large power, short duration of <5ms, and an especially high dispersion measure of 375 pc/cm^3. The astronomical community was initially skeptical, some explaining the data as interference.

But over the last decade, Parkes, as well as other radio observatories, such as the Arecibo Observatory in Puerto Rico, the Green Bank Telescope in West Virginia, the Very Large Array (VLA) in New Mexico [8] and the Australian Square Kilometre Array Pathfinder (ASKAP), have detected many more bursts. There are multiple theories about the origins of FRBs, from supernovae [9] and magnetars [10] to SETI [11], and more.

Only three FRBs have been traced to their origin. It was possible to localise one in 2015 due to its repeating nature - FRB 121102, discovered by Spitler in 2012 [12]. More than a few hundred events have so far been detected from this source. The origin of the 'repeater' has been localised to a dwarf irregular galaxy, about a gigaparsec away, at redshift z = 0.19,

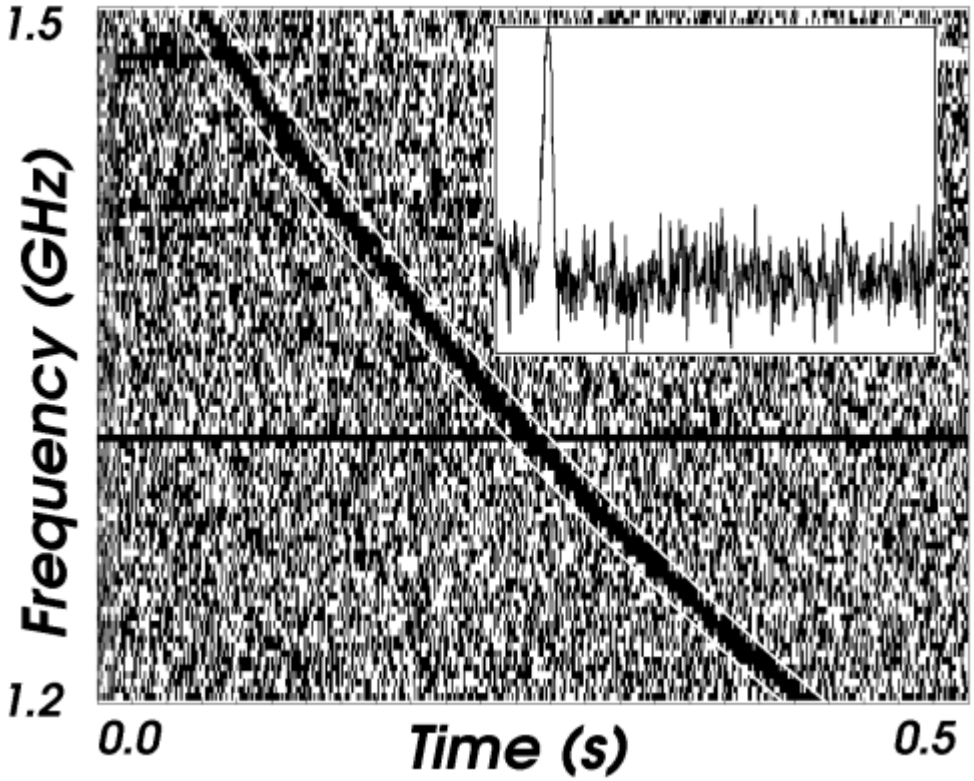

Figure 2: The radio profile of the first Fast Radio Burst, the 'Lorimer burst', near the Small Magellanic Cloud. The inset box is the time sequence of the signal strength at one frequency. The burst was extremely intense, 30 Jy peak flux, and observed across a 288 MHz radio band. The dispersion measure of the FRB was very high, of 375 pc/cm^3, and the large value pointed towards the burst's extragalactic origin [1].

based on an apparent radio flare from that galaxy that lasted several days after the burst [13]. The repeating nature of FRB 121102 has ruled out models that consider the destruction or irreversible transformation of the source, namely stellar collapse, merging binaries and catastrophic collisions - at least for the FRBs of a repeating nature, as it is possible that there are different types of FRBs.

One idea is that the origin of FRB 121102 might be a young, rapidly spinning, highly magnetised neutron star - a magnetar [14, 15]. However, the magnetar model is not without issues: there are magnetars much closer to Earth, but no FRBs have ever been detected from any of them. For example, the magnetar SGR 1806-20 in the Milky Way gave off a giant gamma-ray burst in December 2004, but no FRBs were observed [16].

Another repeating burst was found by CHIME in January 2019, but has not yet been localised. Two back-to-back papers in August 2019 detailed the localisation of two more bursts - both one-off FRBs [17, 18]. One was localised by ASKAP and the other by Caltech's Owens Valley Radio Observatory (OVRO), using the new Deep Synoptic Array-10. Unlike the repeater, these two bursts both come from galaxies with very little star formation, so

the mechanism responsible for their generation might be different from that of FRB 121102. Thus, it is likely that there might be different types of mechanisms generating FRBs. In this work, we propose a model that involves the possibility of some FRBs being triggered by superradiance. This term, which describes a phenomenon involving a low-frequency bosonic wave being scattered from and amplified by a spinning black hole, was coined in 1954 by Dicke [19]. The idea was further developed in the early 1970s by Zeldovich and collaborators in the Soviet Union, and Press and Teukolsky in the US [20].

The necessary condition for superradiance is for the frequency of the incident bosonic wave to be less than the angular velocity of the BH times the azimuthal number, m:

$$\omega < m\Omega \quad , \tag{1.1}$$

where the integer $m \geq 1$ and each m represents a different superradiant mode [21]. Superradiance is most efficient for the $m = 1$ mode and this translates into the condition that the Compton wavelength of the incident wave is comparable to the Schwarzschild radius of the black hole [21]. The wave would then be scattered off the BH's outer region, the ergosphere, and amplified, extracting energy from the black hole's angular momentum and causing the BH to spin down [21].

In a vacuum, amplified massless waves would simply escape to infinity, carrying away only a little of the BH energy. However, in the presence of a confining mechanism, such as that provided by a perfectly reflecting mirror surrounding the black hole, superradiance exhibits an instability since the waves repeatedly scatter and become exponentially amplified [21]. One possible confining mechanism is the interstellar plasma [21], a gas of free electrons and ions. Photons, elementary excitations of the electromagnetic field, are massless particles, but when they propagate in a plasma, they acquire an effective mass due to collisions and interactions with the particles in the plasma [21].

However, photons with a frequency lower than the plasma frequency cannot propagate in the plasma and become 'trapped'. If a black hole resides in a plasma with 'trapped' photons, now considered effectively massive particles, those photons with the lowest modes and with the wavelength of the order of the BH radius will scatter off the ergosphere, and be amplified. The 'mirror' of the plasma will then cause the amplified pulse to bounce back and forth, exponentially increasing in amplitude, and eventually leading to an instability [21] - a bosonic cloud that would eventually collapse with potentially observable results [22].

As the observed frequency of FRBs is a known value of ~ 1 GHz, for such a burst to occur, there would have to be a massive particle of a specific wavelength interacting with a spinning black hole of a radius that is comparable to the effective Compton wavelength of the photon. To generate high FRB frequencies, we need the plasma frequency to be high as well, and we calculate in this paper that such dense plasmas exist in the transition region of stars. Knowing the required plasma frequency, we then determine the mass of the black hole

for which the superradiant instability would occur. For the necessary plasma frequency, we determine that the mass of the black hole should be of the order $10^{-4}M_{\odot}$. Such black holes could thus experience superradiance in the presence of dense plasmas found in the transition region of stars.

Such black hole masses are below that which can be obtained by the collapse of normal baryonic matter through stellar evolution, and thus such a black hole would have to be some kind of a primordial black hole (PBH), such as those that could have appeared in the early Universe from the collapse of scalar field fluctuations [23]. Such black holes are often considered to be a potential cold dark matter candidate [23].

Cosmological measurements have constrained the abundance of dark matter in the Universe to be ∼83% of total mass [24], see Fig. 3. Observations and simulations have greatly improved the understanding of DM distribution in Galactic haloes, but its nature is still unknown. The main dark matter candidate, the weakly-interacting massive particles (WIMPS),

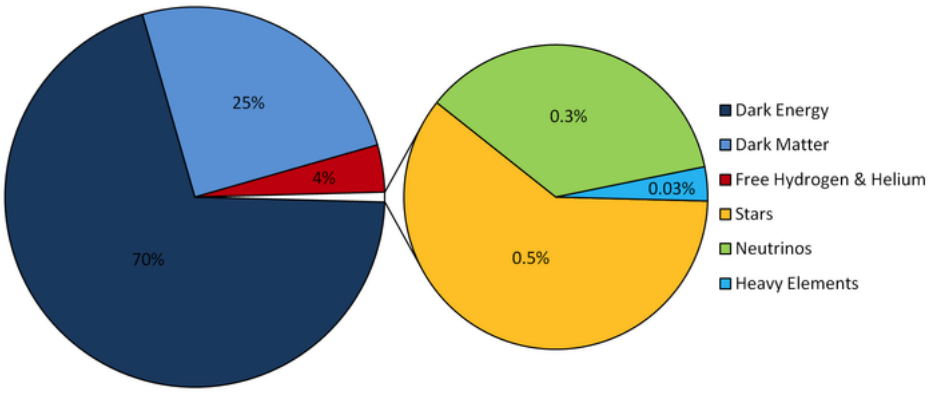

Figure 3: About 70% of the contents of the Universe is dark energy, the rest is mass: 17% of baryons (galaxies, stars, gas) and 83% of dark matter (Credit: Creative Commons).

have still not been detected [25], so other options are also being considered, such as axions [26], sterile neutrinos [27] - and also PBHs. First invoked in the mid-20th century, PBHs were studied by Carr, Hawking, and others [28]. In the 1980s and 1990s, it was suggested that PBHs could be dark matter, having appeared due to inflation, an early period of ultra-rapid expansion of the universe thought to have taken place some 10^{-34} seconds after the Big Bang singularity [29]: quantum fluctuations magnified by inflation could have produced very dense regions that then collapsed, leading to the formation of PBHs less than one second after the end of inflation [30] [31].

On 14 September 2015, LIGO detected the merger of two $\sim$ 30 $M_{\odot}$ black holes, ∼400 Mpc (1.3 billion light years) away [32]. The detection has rekindled interest in PBHs as a dark matter candidate [33] due to the two progenitors being bigger than a typical stellar black hole, and to the weakest constraints on PBHs of $M \sim 10$ - $100M_{\odot}$ corresponding to the progenitors' masses [34]. Various observations, including microlensing, which rely on monitoring a field of

stars and detection of magnification caused by compact objects transiting the line of sight, have provided stringent constraints on the range of masses of PBHs as DM candidate (see Fig. 4). The black holes considered in this work have masses far smaller than those observed by LIGO, but could still provide a fraction of up to 10% of the total dark matter [35], as shown in Fig. 4.

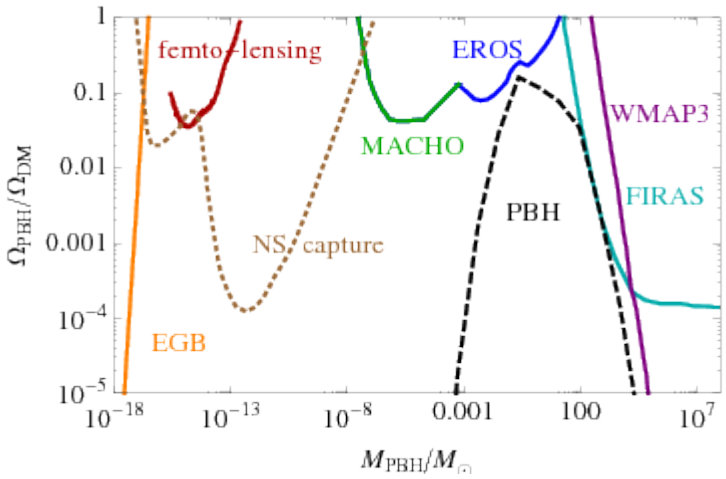

Figure 4: Limits on the abundance of PBH today, from extragalactic photon background (orange), femto-lensing (red), micro-lensing by MACHO (green) and EROS (blue) and CMB distortions by FIRAS (cyan) and WMAP3 (purple). EGB: A constraint due to the fact that tiny PBHs would evaporate because of Hawking's radiation. If they do, they should emit gamma rays at a certain rate, which is incompatible with observations. NS CAPTURE: a neutron star can capture a PBH and, if it does, the PBH can destroy the star by 'swallowing' it. Since it is possible to observe NSs, it is possible to put this constraint on PBHs. Femto-lensing of gamma-ray bursts: Compact objects may induce gravitational femto-lensing of GRBs. The lack of femto-lensing detection in the Fermi Gamma-Ray Burst Monitor experiment has given evidence that in the mass range $10^{-16} - 10^{-13} M_{\odot}$, PBHs cannot account for a large fraction of DM. MACHO/EROS: Microlensing observations. Similar to exoplanet searches, the gravitational field of a PBH would deform the trajectory of light that can be observed by tracking distant stars. BLACK: The PBH region is the one allowed by PBHs in the LIGO band. WMAP3/FIRAS: distortion of the CMB in the presence of PBHs. Figure from Clesse et al. [36].

In this work, we propose that photons in the stellar transition region (having an effective mass induced by the plasma) could scatter off spinning, nonevaporating PBHs of $\sim 10^{-4} M_{\odot}$ and trigger superradiant instabilities in the form of detectable radio bursts in the frequency range conforming to the observed FRBs. We calculate the rate of FRBs in the Universe, assuming that superradiant bursts can occur from the interaction of photon plasma with PBHs in the transition region of stars, and compare this to observations. According to various estimates, FRBs may be occurring as frequently as every second in the Universe [37]. We, however, calculate the rate to be 184 FRBs a day - making FRBs produced via

this mechanism a viable possibility, but one that wouldn't be able to account for all FRBs thought to occur in the Universe.

The thesis is organised as follows:

- In Section 2, we start by giving the theoretical and observational background to the work, followed by the results from N-body simulations and observations on which our calculations are based.
- In Section 3, we first calculate the number density of stars and PBHs in a typical galaxy, then calculate their collision rate, and finally extrapolate the rate to the observable Universe using a typical halo mass function (HMF).
- In Section 4, we discuss the results, the challenges for the model and make suggestions for further work.

2 THEORETICAL AND OBSERVATIONAL BACKGROUND

2.1 FRBs: Current observations

All known FRBs are characterised by high dispersion measures of $\sim$ 200 - 3000 pc/cm^3, which suggest extragalactic origins ($\sim$ Gpc) [38]. They are also of ultra-short $\sim$ ms-long duration [38].

Estimates of the occurrence rate of FRBs in the observable Universe vary. The actual number depends greatly on the sensitivity threshold of a particular radio telescope. While 34 FRBs have been found over the past decade (at the time of writing) [34], the detection rate has been rising thanks to the improving sensitivity of telescopes and more instruments purposefully searching for the bursts. Between 2007 and 2012, one FRB was detected, but in the years 2013 to 2017 there were a few found per year, and in October 2018, observations by ASKAP found 20 [34].

However, the occurrence rate of FRBs in the observable Universe is estimated to be much higher. Fialkov and Loeb estimate the rate of FRBs observable by future telescopes to exceed one FRB per second per sky when accounting for faint sources [37]. They assume that the repeating FRB 121102, which resides in a metal-poor dwarf galaxy, represents the entire FRB population, and consider frequencies between 50 MHz and 3.5 GHz. Other estimates are more conservative. Crawford et al. analysed three Parkes multibeam 1.4 GHz surveys for the presence of FRBs [1]. The surveys observed the Magellanic Clouds and unidentified gamma-ray sources at mid-Galactic latitudes for new radio pulsars, and had a combined total of 719 hr of Parkes multibeam on-sky time. The paper adds this duration to the on-sky time (7512 hr) from the five Parkes surveys analysed by Rane et al., and for the frequency of 1.4 GHz obtain the rate of 3.3×10^3 events per day, for redshift z = 1 [39].

In this work, we propose that one possible mechanism for FRB production could be via superradiant instabilities occurring during the collisions of stars and PBHs. We calculate the rate of events which could be expected, and compare this to the observational figures described here.

2.2 Superradiance in plasma

Photons can propagate in interstellar environments within a galaxy or a galaxy cluster as long as their frequency is above the plasma frequency, which depends on the plasma density. When the photon is able to propagate, it acquires an effective mass given by the plasma frequency [21].

Pani and Loeb [35] analysed nonevaporating PBHs with masses greater than 10^{-18} solar masses, with further constraints on the dark matter fraction in the range $M > 10^{-8}M_{\odot}$. They showed that as superradiant instabilities can be caused by effectively massive photons propagating in plasma, and estimated the upper bounds on the dark matter fraction in spinning PBHs. Conlon and Herdeiro [22] studied the possibility of FRBs being generated by spinning stellar black holes in a photon plasma. They considered black holes with masses $M = 1 - 100M_{\odot}$, which exhibit superradiant instabilities when surrounded by photons with effective masses of $\mu = 10^{-10} - 10^{-12}$eV - which match the plasma-induced photon mass in diffuse galactic or intra-cluster environments [22].

If photons have frequencies below the plasma frequency $\omega < \omega_{pl}$ in any given region, they will be reflected by the plasma and if they start close to the black hole, they will remain close to the horizon. When confined by the plasma just outside the event horizon of a spinning black hole, in the ergosphere region where light co-rotates with the black hole, they will undergo superradiant amplification [21]. An incident low-frequency wave will scatter off the black hole with more total energy than it originally had, at the expense of the black hole's angular momentum. The energy boost will generate more photons, and because of the 'mirror effect' of the plasma, the amplified waves will bounce off the plasma and, in a runaway process, keep interacting with the black hole, creating a 'bosonic cloud' around it [21].

When the bosonic field grows, it may become unstable due, for example, to self interactions in the field or the black hole moving into a region where the plasma frequency decreases. It may then collapse in on itself and emit a burst of electromagnetic radiation, analogous to the stellar collapse leading to a supernova. Conlon and Herdeiro thus suggest [22] that rotating stellar black holes are unstable to formation of a photon cloud, at the instability timescale of milliseconds.

As galactic plasma frequencies correspond to long-wave radio frequencies of 10^{-10}eV, equivalent to 24kHz, it might be possible, the authors argue, to observe such a rapid energy transfer in radio frequencies, as ultra-rapid flashes in the form of FRBs [22]. The short timescale is due to the exponential nature of superradiance - the rate of energy release is exponentially growing, akin to a pulse.

As superradiance is known to be a repetitive phenomenon, this could in addition explain the repeating nature of some (at least one known) FRBs.

A potential problem with the work of Conlon and Herdeiro is that the radiation frequency the authors obtain is very different from the observed frequencies of FRBs. They find 24 kHz while $\omega_{FRB} \sim 1$ GHz. Motivated by their work, we propose a similar mechanism which would instead result in the observed frequency of ~ 1 GHz.

2.3 Determining the necessary black hole size for superradiance to trigger FRBs of the observed frequency

Obtaining the necessary plasma frequency to have the observed frequency of FRBs would necessitate an electron number density of $n_e \approx 10^{-9}\omega_{FRB}^2 \mathrm{cm}^{-3} \approx 10^9 \mathrm{cm}^{-3}$:

$$\omega_{pl} = \left(4\pi\alpha \frac{n_e}{m_e}\right)^{1/2}, \tag{2.1}$$

where $\alpha = \frac{e^2}{4\pi c \epsilon_0 \hbar}$ is the fine structure constant.

The diffuse galactic free electron density varies from around $n_e \sim 10 \mathrm{cm}^{-3}$ in the inner ~ 50 pc of the galaxy, through $\sim 4 \times 10^{-2}$ cm^{-3} near our solar system, falling away rapidly as one moves vertically away from the disk. We know that it is the transition region of stars that corresponds to the electron number density of this order, as shown in the example of our Sun [40]. We calculate the wavelength:

$$\omega_{pl} = \omega_{FRB} = 10^9 \mathrm{s}^{-1} \tag{2.2}$$

$$10^9 \mathrm{s}^{-1} \frac{G}{c^3} = 0.247 \times 10^{-26} \mathrm{kg}^{-1} \tag{2.3}$$

$$\lambda = \frac{1}{\omega_{pl}} = 4 \times 10^{26} \mathrm{kg} \approx 2 \times 10^{-4} M_\odot \tag{2.4}$$

We set $G = c = 1$ in geometric units. Having determined the plasma frequency - and hence the frequency of the incident photons - we now have the wavelength λ. Using the superradiant condition, we know that a BH in this plasma has to have a radius of the same order, $r_S = \frac{2GM}{c^2}$. We then calculate the necessary mass of the black hole:

$$\lambda = r = 2m_{BH} = 2 \times 10^{-4} M_\odot \tag{2.5}$$

$$m_{BH} = 10^{-4} M_\odot \tag{2.6}$$

The mass of the black hole in this plasma, therefore, should be around $m = 10^{-4} M_\odot$ in order for the plasma photons to trigger a superradiant instability. And the corresponding radius of such a black hole should be, using the conversion factor of $1 M_\odot = 2 \times 10^{30}$kg=1.5km:

$$10^{-4} M_\odot \Longleftrightarrow 0.15\mathrm{m} \tag{2.7}$$

$$r_{BH} = G \times 2 \times 10^{-4} M_{\odot} = 0.3\text{m} \tag{2.8}$$

Black holes of such a mass cannot be formed by baryonic collapse, and thus must have another origin, for example primordial black holes (PBHs). Such tiny BHs could have formed in the early Universe, when quantum fluctuations magnified by inflation could have generated extremely dense regions which later collapsed, leading to the formation of PBHs less than one second after the end of inflation [30] [31].

There is a range of constraints on PBHs. While Fig. 4 refers to PBH content being about ∼10 % of total dark matter content in the Universe, in [35], Pani and Loeb put constraints on PBHs exhibiting superradiance, determining that the mass of $m = 10^{-4} M_{\odot}$ corresponds to ∼0.2 % of DM being attributed to PBHs, as shown in Fig. 5.

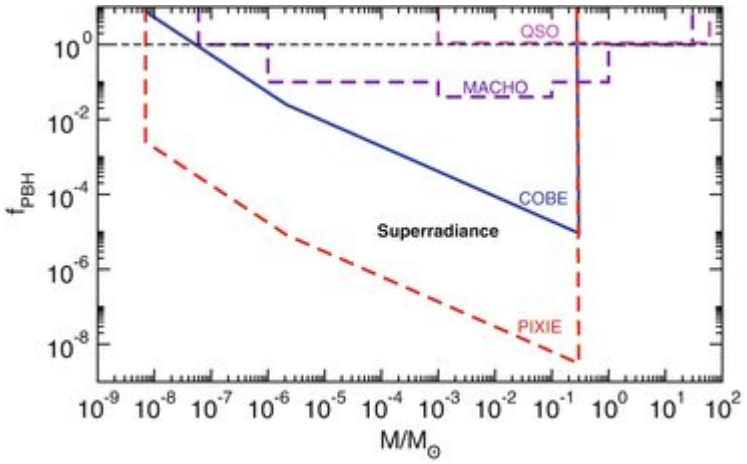

Figure 5: Upper limits on the mass fraction of dark matter in PBHs with masses in the range $10^{-9} M_{\odot} < m < 10^{2} M_{\odot}$. The solid blue curve is the theoretical constraint derived in [35] using COBE/FIRAS data.

They also estimate the instability timescale, calculating the time it takes for superradiance to occur, and show that it is an extremely fast process. To determine the time, they use the following equation:

$$M\tau_{SR}^{-1} \approx \gamma_{Sl}(\tilde{a}m - 2r_{+}\omega_{p})(M\omega_{p})^{4l+5+2S}, \tag{2.9}$$

where r_{+} is the horizon radius, l is the harmonic index of the corresponding mode, N is an integer, $S = 1, -1, 0$ the mode polarisation, and γ_{Sl} is a numerical coefficient. A rearrangement of the equation for τ_{SR} gives us the timescale for the superradiant instability to build up, in terms of the relevant parameters of the BH/boson system. It is inversely proportional to $(\tilde{a}m - (2r_{+}\omega_{p}))$, so when this quantity is zero, τ_{SR} will become very large. We set the values close to the extremal state as the following:

$S = 1$ as photons in plasma have spin 1, $l = m = 1$ (the dominant superradiant mode), $\tilde{a} = 0.99$ (near extremal spin BH - required for max SR), $\gamma = 1$ (a numerical factor, of order

one - as we only want an approximation, we can neglect the exact value), r_+ is the horizon radius, ω_p = plasma frequency, M = mass of our BH = $10^{-4}M_\odot$. To determine the r_+, we use the following formula for fast-spinning black holes [41]:

$$r_H^{\pm} = 1 \pm \sqrt{1 - a^2}, \tag{2.10}$$

where the spin parameter a tends to 1 and where $a = \tilde{a}$ from equation (2.9). The spin parameter is defined as follows: $a = cJ/(GM^2)$, with c the speed of light, J the angular momentum of the black hole, G the gravitational constant and M the mass of the black hole. In our case, for highly spinning black holes, the dimensionless value will be approximately $r_+ \approx 1$.

In [35], Pani and Loeb state that the dimensionless parameter $M\omega_p$ is maximum when $M\omega_p = 0.4$ and for nearly-extremal BHs.

With these values, we use the equation (2.9) to calculate the timescale τ_{SR}, which is roughly the time constant for the superradiant growth - i.e., how long the BH takes to grow the photon cloud. All the quantities are in geometric units. Upon substitution we get:

$$\omega_{pl} = \frac{0.4}{m_{BH}} \tag{2.11}$$

$$r_+ \approx 1 m_{BH} \tag{2.12}$$

$$10^{-4}M_\odot\tau^{-1} = 1 \times (0.99 - 2 \times 0.4)(0.4)^{11} \tag{2.13}$$

$$\tau = \frac{M_\odot}{0.0797} \tag{2.14}$$

Converting the units:

$$\tau = \frac{2 \times 10^{30}\text{kg} \times G}{c^3 \times 0.0797} \tag{2.15}$$

$$\tau = 6.2 \times 10^{-5}\text{s}. \tag{2.16}$$

The very short value of τ demonstrates that the timescales for SR to occur are very short.

2.4 N-body simulations and observational results

2.4.1 NFW profile: The concentration parameter, scale density and scale radius

In this section, we describe the distribution of dark matter in a halo based on N-body simulations. In particular, we describe the relationship between the concentration of the halo and its virial mass. We also demonstrate how the scale density and the scale radius of a halo are obtained.

Approximately 70% of the contents of the Universe is dark energy, the rest is matter, consisting of baryons (galaxies, stars, gas) and dark matter [42]. About 83% of the mass is dark matter and the rest is baryonic [43]. According to N-body simulations, in a halo dark matter starts without stars and the smallest structures form first [44]. During its formation,

a halo becomes virialised, reaching a dynamic equilibrium between the kinetic and potential energy of the constituents: $2T = -V$. The final, virial mass of a halo is also called M_{200}, because, empirically, the equilibrium occurs when the density of the halo is about 200 times the critical density of the Universe. The radius that encloses this mean overdensity of 200 times the critical value, the virial mass, and defines in dynamic terms the border of the halo is the virial radius.

Most dark matter haloes can be completely described by one of the most commonly used model profiles for dark matter haloes called the Navarro-Frenk-White (NFW) profile - a spatial mass distribution of dark matter fitted to haloes identified in N-body simulations by Julio Navarro, Carlos Frenk and Simon White [45]. Typically in DM-only simulations, the dark matter forms profiles with the functional form in accord with the NFW profile:

$$\rho(r) = \frac{\rho_0}{\frac{r}{R_S}(1+\frac{r}{R_S})^2} \ . \tag{2.17}$$

For a dark matter halo of a specific virial mass, there are two unknown parameters, according to the NFW profile: scale radius R_S and scale density ρ_0. There is also another parameter used to describe the shape of the profile, called the halo concentration parameter c: $c(M) = \frac{R_{vir}}{R_S} = \frac{R_{200}}{R_S}$, where R_{vir} is the virial radius [46]. Haloes with higher concentration have almost all the dark matter near the center, and the amount of dark matter decreases radially as a function of R_{vir}. For haloes with low concentrations, the distribution of the mass is more even near the center. For a given virial mass of a halo, we have a specific concentration parameter, which is needed in order to calculate ρ_0 and R_S.

The larger the halo, the lower the concentration of dark matter in it. Relating the virial mass and the concentration will mean that it will no longer be necessary to have both M_{vir} and c to calculate the mass profile of the halo, but only one will be sufficient.

To calculate the concentration parameter, a formula that relates M_{vir} and c, derived in Klypin et al. [47], is useful:

$$c\left(M_{vir}\right) = C_0 \left(\frac{M_{vir}}{10^{12}h^{-1}M_\odot}\right)^{-\gamma} \left(1 + \left(\frac{M_{vir}}{M_0}\right)^{0.4}\right) \ , \tag{2.18}$$

where c is the concentration parameter, h is the dimensionless Hubble parameter $h = 0.7$, and C_0 and M_0 are the parameters for the concentration - mass relation that the authors give for various redshifts.

The authors obtain the formula having performed the MultiDark cosmological N-body simulations (http://www.multidark.org/). To each of the haloes used in the simulations, they assigned the concentration parameter c and the virial mass M_{vir} of the NFW density profile that better matched the distribution of mass density. Then they derived a relationship - a function with three free parameters, which have different values for different redshifts. Their

relationship thus allows to determine with great precision the concentration parameter of a halo, at any redshift, while only knowing the halo's virial mass.

With the known concentration parameter, it is then possible to determine R_S and ρ_0 of a halo by using the following two equations for the virial mass - where equation (2.19) is the integration of the NFW profile, equation (2.17) within the virial radius, and equation (2.20) is the definition of the virial mass:

$$M_{vir} = M_{200} = \int_0^{R_{vir}} 4\pi r^2 \rho(r)\, dr = 4\pi\rho_0 {R_S}^3 \left[\ln(1+c) - \frac{c}{1+c}\right] , \tag{2.19}$$

$$M_{vir} = M_{200} = \frac{4}{3}\pi {R_{vir}}^3 \times 200\rho_{crit} . \tag{2.20}$$

In the second equation, $200\rho_{crit}$ is the overdensity. The critical density of the universe is $\rho_{crit} = \frac{3H_0^2}{8\pi G} = 1.8788 \times 10^{-26} h^2$ kg/m^3, where h is a dimensionless Hubble parameter $h = 0.7$ [48]. Upon substitution, we get $\rho_{crit} = 136 M_\odot$ kpc^{-3}. Now all the ingredients are known to calculate R_S and ρ_0 of any DM halo, and we will proceed with these calculations in subsection 3.1.

2.5 The distribution of the baryonic matter in a halo

While the NFW profile is important to determine the parameters related to dark matter, the baryonic matter must be taken into account as well. To determine the stellar mass of a halo, the following relationship from Ferrero et al. [49] is useful, which relates the total stellar mass M_S and the virial mass of a halo - and which we will use to calculate the stellar mass in subsection 3.2:

$$\frac{M_S}{M_{vir}} = C \left(1 + \left(\frac{M_{vir}}{M_1}\right)^{-2}\right)^{\kappa} \left(\left(\frac{M_{vir}}{M_0}\right)^{-\alpha} + \left(\frac{M_{vir}}{M_0}\right)^{\beta}\right)^{-\gamma} , \tag{2.21}$$

where the various parameters are defined and will be used in our calculations in subsection 3.2.

To derive the formula, the authors relied on a relationship from an earlier paper by Guo et al. [50], which is effectively the right-hand side of (2.21), and introduced an extra term with two free parameters, κ and M_1. Guo et al.'s relationship:

$$\frac{M_S}{M_{vir}} = C \left(\left(\frac{M_{vir}}{M_0}\right)^{-\alpha} + \left(\frac{M_{vir}}{M_0}\right)^{\beta}\right)^{-\gamma} \tag{2.22}$$

In Guo et al. [50], the authors use the Abundance Matching (AM) technique in an N-body simulation to determine which galaxy should reside in which halo. In the simulation, haloes are ranked by mass, from more to less massive ones, and the same ordering is applied to observed galaxies. The mass is inferred from the simulation using the halo mass function

(HMF) of dark matter haloes - a characteristic property of cosmological structure formation models that quantifies the number density of dark matter haloes for a given mass in the Universe [50].

Observationally, the mass of a galaxy can be calculated from the distance and brightness of galaxies determined during surveys such as SDSS [51], throughout a well-defined region of space. Directly determined stellar luminosity of each galaxy is converted into stellar mass by assuming a stellar mass-to-light ratio depending on the galaxy's measured colour. Counting galaxies as a function of mass within the known volume then gives the observed stellar mass function (SMF).

The end result places the most massive galaxies in the most massive haloes, the second most massive galaxies in the second most massive haloes, and so on. And as a halo's mass can also be determined from a galaxy's rotation curve, as it is the additional mass that should be added to the galaxy mass to reproduce the observed rotation speed of the galaxy, the observational results can then be compared to the AM results [50].

Guo et al. [50] used the HMF measured in the simulations, and the SMF taken from published observational papers, many of which were based on observations from the SDSS [51]. They then plotted the obtained values of M_{halo} calculated in simulations vs M_{galaxy} from observations (the black solid line in Fig. 6), using the AM technique: matching the most massive dark matter halo from simulation to the most massive observed galaxy, and so on. They then derived the relationship (2.22) that allows to be determined which mass a galaxy should have to reside in a halo of a given mass. The paper concludes that galaxies with stellar mass exceeding $\approx 10^6 M_\odot$ must reside in haloes with virial mass typically greater than $10^{10} M_\odot$.

While for medium and high mass galaxies AM holds, for low mass galaxies it doesn't seem to, as Ferrero et al. demonstrate in [49]. According to the observed dynamics of the galaxies, galaxies tend to reside in smaller haloes than where they 'should' reside as derived using the AM relationship - i.e., Guo's relationship doesn't hold well for galaxies with low stellar masses. This is the 'too big to fail' problem [52] - with tensions between observations and simulations at dwarf galaxy scales, demonstrating that ΛCDM doesn't work well when it comes to reproducing the properties of observed dwarf galaxies.

Ferrero et al. [49] modified Guo's relationship to account for this discrepancy between observations and simulations, with observations showing that smaller galaxies may reside in haloes smaller than $10^{10} M_\odot$. Ferrero et al. [49] used the observed rotation curves of neutral hydrogen in several galaxies and developed a prediction of the M_{halo} that these galaxies should have according to their dynamics. They also obtained stellar masses of these galaxies from previous papers that they cite in section 2 of [49].

They plotted M_{halo} vs M_{galaxy} together with the curve from Guo et al., Fig. 6. For the values to match, they needed to add an additional term to the Guo's formula with two free parameters, M_1 (the value where Guo's curve starts to change) and κ, which shows how

big this change is. The new relationship means that galaxies with stellar masses lower than $10^8 M_\odot$ should reside in haloes less massive than expected by Guo's relationship. So while Guo's formula holds for large and medium stellar masses, the Ferrero paper emphasises that there are great uncertainties for galaxies with low stellar masses.

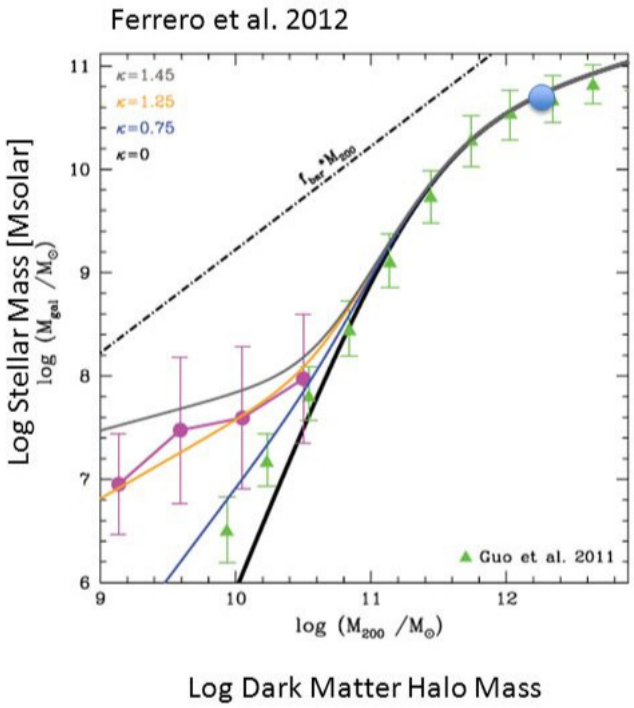

Figure 6: Stellar mass - halo virial mass relation, in the units of solar masses. The black solid line indicates the abundance-matching model of Guo et al. [50] ; solid triangles correspond to the semianalytic model of Guo et al. [53]. The dot-dashed line indicates the total baryonic mass of a halo according to latest estimates of the universal baryon fraction (a cosmological parameter that corresponds to the percentage of baryons (17%) over all the mass in the Universe, ≈ 0.17) The magenta curve shows the average galaxy mass-halo mass relation derived from dwarf galaxies in the Ferrero et al. sample. Circles indicate the average in each halo mass bin. Coloured solid curves correspond to various values of the parameter κ; $\kappa = 0$ corresponds to the abundance-matching relation, higher values correspond to shallower halo mass dependence of galaxy mass. The blue dot is the Milky Way. Figure from Ferrero et al. [49].

2.6 Total enclosed mass: NFW profile and Plummer profile

Integrating the NFW profile (2.17) within some radius r allows one to obtain the mass of dark matter in a halo enclosed within that radius:

$$M_{DM}(r) = 4\pi\rho_0 R_S^3 \left[\ln\left(\frac{R_S + r}{R_S}\right) - \frac{r}{R_S + r}\right] \ . \tag{2.23}$$

In order to obtain the mass of stars within that radius, the Plummer model is useful (equation 2.24) - a density law originally applied by Plummer to fit observations of globular clusters [54]. It is frequently used as a model in N-body simulations of stellar systems, and it relates the density of stars as a function of radius to the stellar mass in a halo:

$$\rho_S(r) = \frac{3M_S}{4\pi a^3} \times \left(1 + \frac{r^2}{a^2}\right)^{-\frac{5}{2}} , \tag{2.24}$$

where a is the Plummer radius, a scale parameter which sets the size of the cluster core. Integrating the expression (2.24) allows to obtain the stellar mass in a halo enclosed in some radius r:

$$M_S(r) = 4\pi \int_0^r r'^2 \rho_S(r')\, dr' = M_S \frac{r^3}{(r^2 + a^2)^{\frac{3}{2}}} . \tag{2.25}$$

The Plummer radius a is calculated to be $a = 0.766 R_{\frac{1}{2}}$, where $R_{\frac{1}{2}}$ is the half-light radius, also known as the effective radius of a galaxy - the radius that encloses half of the total light observed from a galaxy. To obtain the half-light radius $R_{\frac{1}{2}}$, a useful relationship between the stellar mass and the stellar radius in a halo is derived in Ichikawa et al. [55]:

$$\log_{10} R_{\frac{1}{2}} = b_r(\log_{10} M_S - M) + \log_{10} R^M_{\frac{1}{2}} , \tag{2.26}$$

where M_S is the stellar mass and M is a parameter, which is for star-forming galaxies is $M = 10$. The authors give the values of $b_r = 0.111$ and $\log_{10} R^M_{\frac{1}{2}} = 0.477$.

In this paper, the authors used observational data from galaxies and analysed the relationship between the mass of a galaxy and a certain characteristic radius - either the half-light radius (r_{50}) or the radius that encloses 90% of the total light observed from the galaxies (r_{90}). The aim was to analyse how the increase in mass in galaxies affected their size. According to the Big Bang model, about 300,000 years after the Big Bang, the universe contained only homogeneous hydrogen [56]. After about 14 billion years, it is no longer the case: there are dense galaxies, filaments of gas connecting them, and voids with very low density in gas [56]. The current theory is that galaxies start small and increase in mass with time [57].

The authors used the K-band selected catalogue from the MOIRCS Deep Survey (MODS), carried out with Multi-Object Infrared Camera and Spectrograph mounted on the Subaru telescope in the GOODS-North region (extremely deep observations from NASA's Great Observatories) [58] - a dataset of the galaxies in a field imaged in the K-band, the near-infrared region of the spectrum. They defined the half-light radius as the radius of a circular aperture, starting from the centre of each galaxy and creating a circle of increasing radius, encircling half the K-band light emitted by the galaxy. Beyond a certain radius, the total light within the aperture stops changing, even for larger radii: this is the 'total' light of the galaxy.

Knowing the total light, the authors estimated the radius that contained half of that

light. They used SExtractor software, a program used in observational astronomy to detect galaxies within images and measure their properties [59], to get the r_{50} and r_{90} radii based on the necessary fractions of the total light of a galaxy that the software measured. To get the stellar mass of the MODS samples, the authors referred to results from an earlier paper by Kajisawa et al. [60]. In that paper, Kajisawa et al. performed the Spectral Energy Distribution (SED) fitting technique - a process of fitting colours to estimate specific properties of galaxies. They used the known stellar spectra of individual stars, classified in various types, and assumed a Single Stellar Population with varying proportions of the stellar types. They also assumed a specific evolution for this population. Using the total light from the galaxy in different colours, they constrained these assumptions and fitted them with the observed colours to obtain estimates of the stellar mass in the samples [60].

Ichikawa et al. [55] selected a sample of galaxies from Kajisawa et al. [60] - those that had a measurement in the K-band (most distant, due to redshift). They then used a relationship between the observed light and the stellar mass content of the galaxy and the half-light radius to estimate the 'half-mass' radius in order to determine how mass is distributed between galaxies. They classified the galaxies by redshift and analysed how the half-light-to-mass radius changes with time, moving towards the early Universe. They found that the build-up of mass in galaxies (their total stellar content) is not dependent on mass - all galaxies seem to increase their mass in a similar manner, regardless of their size. The authors conclude that there is no strong evidence for the size evolution at a specific mass over the redshift change.

To derive equation (2.26), the authors plotted the masses of galaxies as a function of the characteristic radius, and fitted a line that adjusts the observational values on the logarithmic scale.

Knowing the half-light radius determined in this way allows to calculate the total stellar mass in a halo, enclosed within this half-light radius. In subsection 3.3, we will use the equations (2.23) and (2.25) to obtain the total mass in any halo, enclosed within the half-light radius.

3 CALCULATION OF FRB RATE IN THE UNIVERSE

Here, we will detail our calculations that lead to the determination of the rate of FRBs in the observable Universe. A brief roadmap of the section:

- First, we will use equation (2.18) to calculate the concentration of a DM halo, along with its two free parameters, the scale density and the scale radius. We will plot the

relationship between the concentration parameter and the virial mass of a halo, and show that the larger the halo, the smaller its concentration.

- Next, we will use equation (2.21) to find the relationship between the virial mass of a halo and the stellar mass, and plot it. We will show that the stellar mass increases with the increasing virial mass.

- We will then calculate the total mass enclosed in a halo, by integrating the equations describing the NFW profile and the Plummer model, equation (3.3).

- Then we will find the average velocity of PBHs in a halo, and use it to calculate the collision rate of PBHs and stars in a halo, equation (3.8).

- Finally, we will find the rate of FRBs in the entire (observable) universe, up to redshift z = 2, by deriving an expression from a plot of a halo mass function.

- We will assume the spin parameter a=1 for all PBHs and we will assume that 100% of dark matter is composed of PBHs for all our calculations. We will discuss what this means for the rate as well as how the rate diminishes if we instead assume that only use a small fraction of dark matter can be composed of PBHs in the next section, Conclusion and Discussion.

3.1 Calculating the concentration parameter, the scale density and the scale radius

First, we need to find c, R_S and ρ_0 for any dark matter halo. We need to obtain the rate of FRBs in today's Universe, hence, we use the values from [47] for the equation (2.18) at z = 0, $h = 0.7$, $M_\odot = 1$, $C_0 = 7.4$, $\gamma = 0.12$, $M_0 = 5.5 \times 10^5 \times 10^{12} h^{-1}$:

$$c(M_{vir}) = 7.4 \left(\frac{M_{vir}}{10^{12} \times 1.43} \right)^{-0.12} \left(1 + \left(\frac{M_{vir}}{M_0} \right)^{0.4} \right) . \tag{3.1}$$

Knowing M_{vir} and c allows to determine the exact distribution of the mass in a specific halo. For instance, for a halo of $M_{vir} = 10^6 M_\odot$, we get $c = 40.54$. Now that we have the concentration parameter, we can solve our two equations and find the density. We set the two equations equal to each other and solve for $\rho_0 = 2.196 \times 10^8 M_\odot$ kpc^{-3}.

We then get $R_S = 0.051$ kpc. In our plot, Fig. 7, we can clearly see that the smaller the halo, the larger its concentration.

In the figure, we obtain a straight line due to the fact that even though there are two power laws in equation (3.1), the first term dominates because the ratio in the second term should be very small compared to 1.

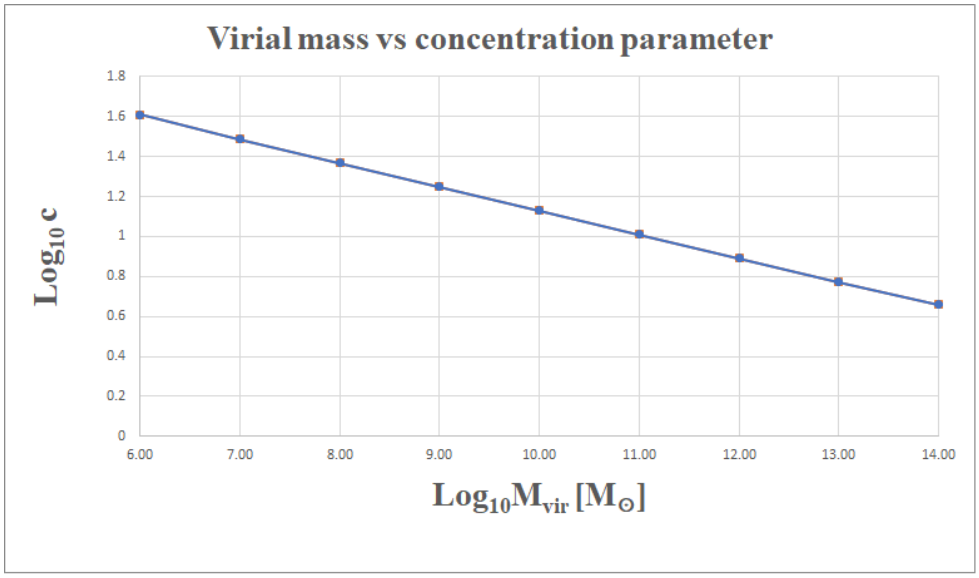

Figure 7: Virial mass of a halo vs concentration parameter, obtained using equation (2.18). Smaller haloes have larger concentrations than larger haloes.

3.2 Calculating the stellar mass of a halo

To obtain the stellar mass of a halo, we use equation (2.21) from Ferrero et al. [49], in order to account for the whole range of galaxy masses, including the low-mass dwarf galaxies. We substitute the values provided in the paper: $C = 0.129$, $M_0 = 10^{11.4} M_\odot = 2.51 \times 10^{11}$, $M_1 = 10^{10.65} M_\odot = 4.47 \times 10^{10}$, $\alpha = 0.926$, $\beta = 0.261$, $\gamma = 2.440$, $\kappa = 0, 0.75, 1, 1.25$, $M_\odot = 1$. We use $\kappa = 1.25$ as this is the value that best adjusts the magenta median curve in Fig. 6 that corresponds to the observational data the authors analyse, and obtain:

$$\frac{M_S}{M_{vir}} = 0.129 \left(1 + \left(\frac{M_{vir}}{10^{10.65}}\right)^{-2}\right)^{1.25} \left(\left(\frac{M_{vir}}{10^{11.4}}\right)^{-0.926} + \left(\frac{M_{vir}}{10^{11.4}}\right)^{0.261}\right)^{-2.440} . \quad (3.2)$$

So for our sample halo of $M_{vir} = 10^6 M_\odot$, we get $M_S = 3.4 \times 10^4 M_\odot$. For the Milky Way, $M_{vir} = 10^{12} M_\odot$, we obtain $M_S = 3.48 \times 10^{10} M_\odot$, a stellar mass that is comparable to other recent estimates such as [61].

In our plot, Fig. 8, it is clearly seen that the stellar mass increases with the increasing halo mass - and the values we obtain correspond to those in Ferrero et al. [49].
In this figure, the form of the plot is explained as follows. There is a transition at around $10^{11.4}$, and that is due to the fact that when $M_{vir} < M_1$, the first term of the equation (3.2) dominates over the second term. When $M_{vir} > M_1$, however, the second term dominates.

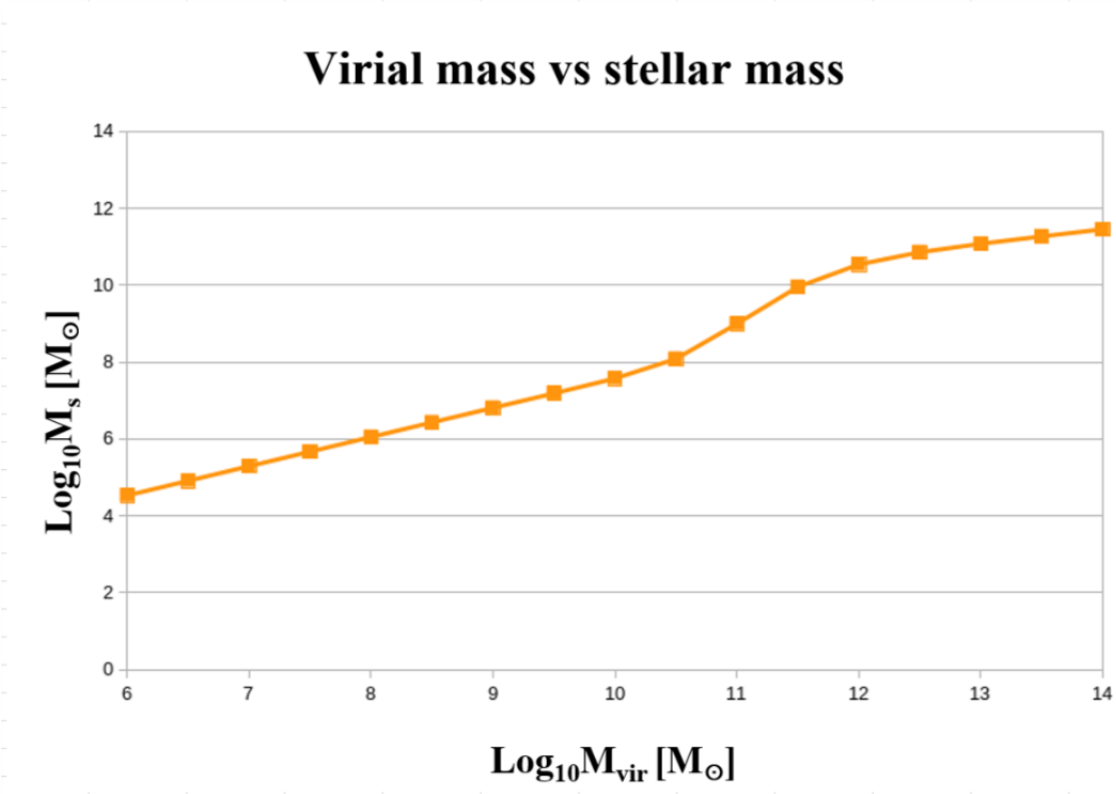

Figure 8: Virial mass of a halo vs its stellar mass, obtained using equation (3.2)

3.3 Calculating the total mass enclosed in a halo

Having determined how the stellar mass varies depending on the virial mass of a halo, it is necessary to obtain the total enclosed mass of dark matter and stars inside a halo, at a specific radius. For that, we use equations (2.23) and (2.25): we integrate the NFW profile to the half-light radius to get the dark matter mass within that radius, and then add to it the total mass of the stars within that radius, which we obtain using the Plummer model:

$$M_{encl}(r) = \left(4\pi\rho_0 R_S^3 \left[\ln\left(\frac{R_S + r}{R_S}\right) - \frac{r}{R_S + r}\right]\right) + M_S \frac{r^3}{\left(r^2 + \left(0.766 R_{\frac{1}{2}}\right)^2\right)^{\frac{3}{2}}} \,. \tag{3.3}$$

We use equation (2.26) to calculate the half-light radius, using the following values given in [55] for star-forming galaxies for low redshifts 0.25<z<0.5: $M = 10$, $b_r = b_{50} = 0.111$, $\log_{10} R_{\frac{1}{2}}{}^M = 0.477$. Substituting the numbers, we obtain:

$$\log_{10} R_{\frac{1}{2}} = 0.111(\log_{10} M_S - 10) + 0.477 \,. \tag{3.4}$$

As M_{vir} is our input, we can find M_S, and hence calculate $R_{\frac{1}{2}}$ and plug it into the equation (3.3) to get the total mass in a halo, enclosed with the half-light radius. To summarise, we

list the values obtained in Table 1.

3.4 Calculating the average velocity of PBHs in a halo

Dark matter as PBHs in a halo will be travelling with a certain velocity, above which it will be able to leave the halo. We need to calculate this maximum velocity of PBHs, the escape velocity v_{EscPBH}, and then we will take half of that for the average velocity of PBHs in the halo. To get the escape velocity at half-light radius, using the NFW profile, we integrate the work done Fdr from $R_{\frac{1}{2}}$ to R_{vir}:

$$\frac{1}{2}m_{PBH}v_{escPBH}^2 = \int_{R_{\frac{1}{2}}}^{R_{vir}} F\,dr = \int_{R_{\frac{1}{2}}}^{R_{vir}} \frac{GM_{encl}m_{PBH}}{r^2}\,dr \tag{3.5}$$

where the total enclosed mass was obtained in the previous section, as given by equation (3.3).

We substitute the values for our sample halo of $M = 10^6 M_\odot$:

$R_{vir} = c \times R_S = 40.54 \times 0.051 = 2.068$, $M_S = 34246$, $R_{\frac{1}{2}} = 0.74$. Knowing that the gravitational constant $G = 4.302 \times 10^{-6}$ kpc $M_\odot^{-1}$ $(\mathrm{km/s})^2$, we calculate the escape velocity of PBHs for this halo: $v_{escPBH} = 2.48\mathrm{km/s}$.

We will use half of the escape velocity in our calculations of the collision rate - the approximate average velocity $v_{av} = 1.23\mathrm{km/s}$ of PBHs in a halo, in subsection 3.5.

3.5 Calculating the number density of stars in a halo

We need the number density of stars $n_S(r) = \frac{\rho_S(r)}{M_\odot}$, which we get using the Plummer model, equation (2.24):

$$\rho_S(r) = \frac{3M_S}{4\pi a^3} \times \left(1 + \frac{r^2}{a^2}\right)^{-\frac{5}{2}} . \tag{3.6}$$

We use it to calculate the mean free path:

$$\lambda(r) = \frac{1}{\pi {r_\odot}^2 n_S(r)} = \frac{4}{3} \times \frac{M_\odot}{M_S} \times \frac{a^3}{r_\odot^2} \left(1 + \frac{r^2}{a^2}\right)^{\frac{5}{2}} , \tag{3.7}$$

where $r_\odot$ is the solar radius. We then use the mean free path, in km, to calculate the collision rate of primordial black holes with stars, in seconds:

$$\Gamma(r) = \frac{v_{av}}{\lambda(r)} , \tag{3.8}$$

where v_{av} is the average velocity of the PBHs, and $v_{av} = \frac{1}{2}v_{escPBH}$, as defined above.

3.6 Calculating the number density of PBHs in a halo

Using the NFW profile and knowing that for our sample halo of 10^6 solar masses $\rho_0 = 2.196 \times 10^8 M_\odot \text{kpc}^{-3}$ and $R_S = 0.051\text{kpc}$, we calculate the number density of dark matter in this halo, n_{PBH}, keeping the mass of one PBH as a free parameter:

$$n_{PBH}(r) = \frac{\rho_{PBH}(r)}{m_{PBH}} = \frac{2.196 \times 10^8 \frac{M_\odot}{kpc^3} \times 0.051\text{kpc}}{r(1 + \frac{r}{0.051\text{kpc}})^2} \times \frac{1}{m_{PBH}} \ , \tag{3.9}$$

3.7 Collision rate per halo

To calculate how often PBHs would collide with stars in a halo, we integrate:

$$\Gamma_{halo} = \int_0^{R_{vir}} \Gamma(r) n_{PBH}(r) \times 4\pi r^2 \, dr \ . \tag{3.10}$$

For our sample halo of $M = 10^6 M_\odot$, we get $\Gamma_{halo} = 1.173 \times 10^{-27}$collisions/second $\times \frac{1}{m_{PBH}}$. As evident from Fig. 9, the larger the halo, the higher the collision rate.

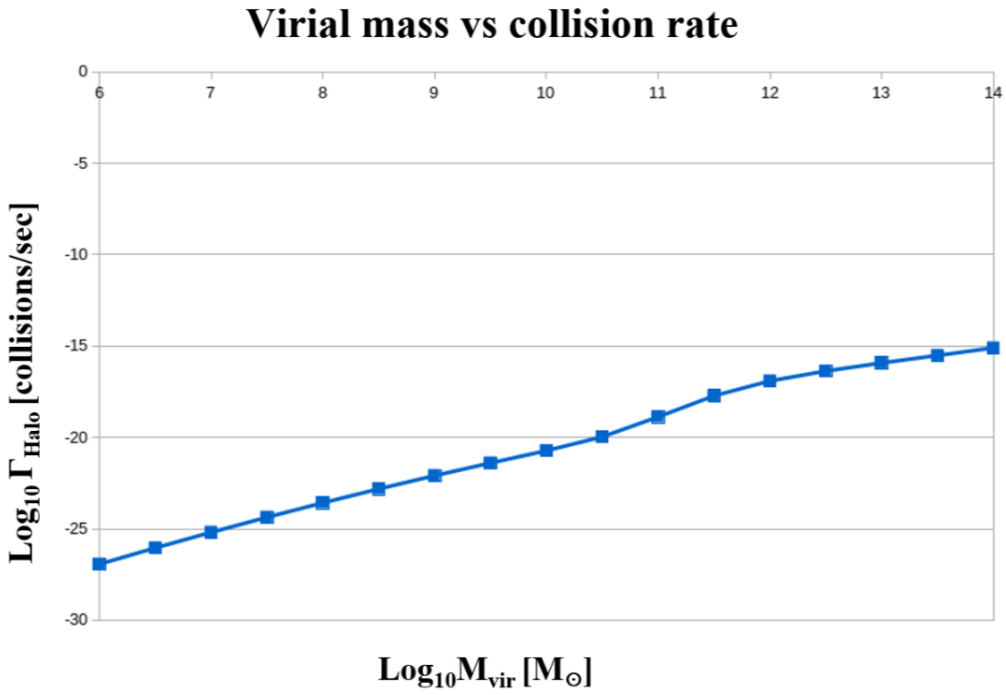

Figure 9: Collision rate of PBHs and stars vs virial mass of a halo.

As expected, we find a transition in Fig. 9 between two regions for the value of $M_{vir} = 10^{11}$. In Table 1 we list the key values we obtain, with the virial mass of the Milky Way $M \sim 10^{12} M_\odot$.

M_{vir}	c	ρ_0	R_s	R_{vir}	v_{av}	Γ_{halo}
1.00E+06	40.5396	2.20E+08	0.0508824	2.06275	1.23538	1.17E-27
1.00E+07	30.7533	1.06E+08	0.144507	4.44406	3.54084	6.46E-26
1.00E+08	23.3303	5.16E+07	0.410387	9.57445	9.15535	2.66E-24
1.00E+09	17.7008	2.54E+07	1.16535	20.6275	21.8024	8.09E-23
1.00E+10	13.443	1.26E+07	3.30831	44.4406	48.3843	1.89E-21
1.00E+11	10.2007	6.39E+06	9.38608	95.7445	103.504	1.33E-19
1.00E+12	7.75839	3.30E+06	26.5874	206.275	241.981	1.22E-17
1.00E+13	5.92418	1.75E+06	75.0157	444.406	472.781	1.18E-16
1.00E+14	4.56795	9.64E+05	209.601	957.445	902.519	7.81E-16

Table 1: The variation of the collision rate of PBHs as well as other parameters with different values of the virial mass.

3.8 FRB rate for the observable universe

In order to obtain the number of haloes of a given mass (M_{vir}) inside a cubic megaparsec, to calculate how many times there will be a collision, we use the halo mass function (HMF). A HMF is a mass distribution of dark matter haloes - the number of haloes of different mass in the universe. It is used in many studies, and we take one from a paper by Marsh and Silk [62], Fig. 10. The vertical axis is the number of haloes and the horizontal axis is total mass. We fit the plot to get a relationship we will use to determine the total number of PBH collisions with stars.

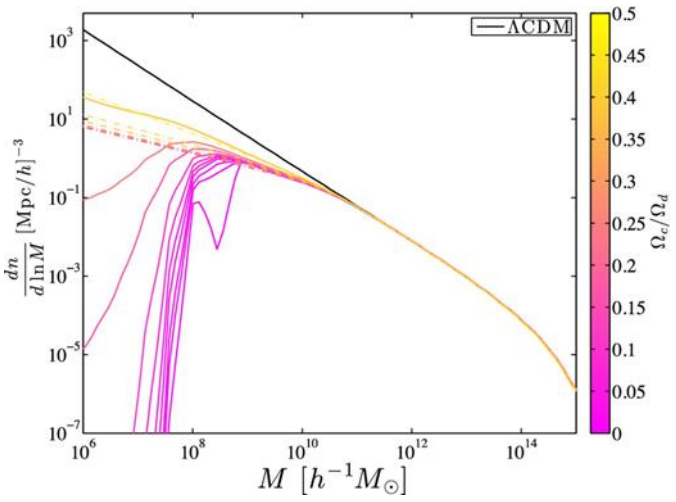

Figure 10: Halo mass function computed directly from CAMB - Code for Anisotropies in the Microwave Background - for ΛCDM by D. J. E. Marsh and J. Silk [62].

We obtain the following relationship by fitting to the black line in Fig. 10:

$$\frac{dn}{d\ln M} = M^{-0.9} \times 10^{8.7} \ , \tag{3.11}$$

where M is dimensionless.
Using the units in the Fig. 10:

$$\frac{dn}{d\ln M} = \left(\frac{M}{M_\odot h^{-1}}\right)^{-0.9} \times 10^{8.7} \times \left(\frac{\text{Mpc}}{h}\right)^{-3} . \tag{3.12}$$

We integrate between $M_{vir} = 10^6 M_\odot$ and $M_{vir} = 10^{15} M_\odot$ to obtain the number of collisions in each cubic Mpc of the universe:

$$\Gamma_{Mpc} = \int_{10^6}^{10^{15}} \frac{dn}{dM} \times \Gamma_{Halo}(M_{vir})\, dM_{vir} = 3.9 \times 10^{-19} \frac{\text{collisions}}{\text{Mpc}^3 \times \text{sec}} \times \frac{1}{m_{PBH}} . \tag{3.13}$$

The radius of the observable universe is 14×10^3 Mpc, but we will use the radius up to z = 2 to account for the maximum number of galaxies: $r = 5066$ Mpc.

As shown in the section on superradiance, subsection 2.3, the mass of a PBH has to be $\sim 10^{-4} M_\odot$ for a superradiant instability to occur, in order for an FRB of the observed frequency of $\sim$ 1GHz to be generated. In the equation (3.9) where we calculated the number density of dark matter in a halo, we left m_{PBH} as a free parameter - and we did the same in the equation (3.13) where we calculated the rate of collisions in one Mpc. Hence, in order to account for the specific mass of $m_{PBH} = 10^{-4} M_\odot$, we have to divide the rate by this mass.

We thus obtain, in the Universe up to z = 2 (which corresponds to the comoving radial distance of about 5066.0 Mpc) and for $m_{PBH} = 10^{-4} M_\odot$:

$$3.9 \times 10^{-19} \times \frac{4\pi}{3} \times 5066^3 \times \frac{1}{10^{-4}} = 0.00212 \text{ collisions/sec} = 184 \text{ collisions/day}. \tag{3.14}$$

4 CONCLUSION AND DISCUSSION

In this work we have calculated the rate of FRBs that would be expected from superradiant effects arising from the collisions of stars and PBHs as 184 events per day. The key assumptions are that PBHs of mass 10^{-4} solar masses make up the majority of the dark matter in galaxies.

However, it is unlikely that so much dark matter would be in the form of PBHs, based on various constraints, as summarised in Fig. 4 in section 2.1. At most, for PBHs of this mass $m = 10^{-4} M_\odot$, we can expect them to constitute $\sim$ 10% of all dark matter in the Universe, according to Fig. 4, and according to Fig. 5, it is even lower, of $\sim$ 0.2% . That means that our result would then be at most about 18 FRBs a day. And the rate should also be reduced further if only a fraction of PBHs have $a = 1$.

That is quite low, compared to other estimates of the rate of FRB events in the Universe. Estimates vary greatly, but a recent paper that analyses the Parkes survey estimates the number in the local Universe (z = 1) to be about 3000 events per day [63]. Another study estimates as much as 1 FRB event happening every single second in the Universe [37].

However, based on the number of FRBs observed so far (about 75 at the time of writing, with the vast majority detected in 2018 and 2019), the detected values are about 5 per year on average, not taking 2018 and 2019 into account. Our result does agree with the detection rate - but is insufficient to explain the much-higher rates estimated in other papers.

One major reason for the discrepancy is the fact that the mechanism producing FRBs is still unknown - and it seems, from the detection of a single repeating FRB and many more non-repeating ones, that there might be different processes triggering these bursts. In this case, PBHs passing through the transition region of stars and triggering observable FRBs via superradiance could account for some of the FRBs in the Universe - while the rest of the bursts would be generated by a different mechanism.

One key assumption of our model is that a certain fraction of PBHs can be dark matter. This assumption could be challenged by a number of papers that rule out PBHs as dark matter for any mass range. Low mass PBHs below the mass of an asteroid would have evaporated by now. In the paper by Loeb and Pani [35] the masses between asteroid and the moon as well as masses between the moon and Earth have also been ruled out. Microlensing rules out masses up to a few solar masses. And in a recent paper [64] Koushiappas and Loeb ruled out masses of tens of solar masses based on the dynamics of dwarf galaxies. Even higher masses are ruled out by other considerations, as shown in [65].

Also, we use a specific value for the mass of PBHs for superradiance to occur, i.e. $m = 10^{-4} M_{\odot}$. But superradiance doesn't occur for exactly one mass corresponding to a specific value of plasma frequency. There will be a certain range of masses and plasma frequencies in which superradiance can occur, which will depend on physical processes that are not yet well understood. This has to be studied further in the future.

Additionally, there are uncertainties arising from a number of values we obtain in our calculation of the rate, such as the uncertainty regarding the halo mass function, the enclosed mass, the virial radius, and others.

This calculation doesn't include the fact that if the velocity dispersion is smaller, it will be easier to capture black holes onto stars through gravitational effect, which isn't taken into account. For a black hole flying past a star at slow enough velocity, it will get attracted to the star and fall onto it. We ignore this in present calculation.

We have also extrapolated the stellar mass vs the virial radius relationship down to very very low mass halo. However, it is still not clear how valid it is for very low masses.

Future work should focus on obtaining more accurate estimates of the expression derived from a halo mass function, as well as better estimates of the PBH dark matter fraction, and other parameters.

In addition, more work should be done on confirming that superradiance can indeed occur in the transition region of stars colliding with PBHs. For that, full numerical modelling of the process using numerical relativity (NR) should ideally be used. However, such simulations will inevitably be very challenging due to the relatively long timescales on the superradiant

process, in units of the BH radius, the relative sizes of the star and the BH, and the lack of symmetry in the collision. So far, the only similar simulations have enforced axial symmetry.

It will also be very valuable to improve the values of the rate of detected FRBs. It will likely be possible in future, with the development of multi-dish radio telescopes. For instance, the Square Kilometer Array will have collecting area of 106 m^2 [66], superseding greatly that of Arecibo and five times that of recently completed Chinese radio telescope FAST [67]. Then there are smaller telescopes, so-called light buckets, such as CHIME in Canada that has recently been completed [7]. CHIME has already started operating, pulling in radio waves from huge regions of space, and has detected 13 new FRBs. Such developments should lead to the observation of many more fainter FRBs. ASKAP and OVRO's Deep Synoptic Array-10 should localise more soon one-off FRBs, as well as the VLA in the future, using a feature called Realfast [8].

To verify observationally whether PBHs can trigger FRBs, more data about the precise localisation of FRBs and their environment is needed. It would be very valuable to detect an FRB in the Milky Way galaxy because it would be billions of times brighter than an FRB at cosmological distances.

To conclude, we find that even with the most generous assumptions, the rate of FRBs cannot be fully accounted for by the PBH as their source alone, and whilst this is a plausible source of FRBs, it cannot be the only one. However, it is important to say that the number of collisions we find is highly sensitive to the input values we take. It therefore means that there is fine-tuning that is currently not understood. We hope to better understand it in future work.

5 ACKNOWLEDGEMENTS

I would like to thank my husband Tim Weber for supporting me throughout the years of my studies at King's College London, without whom I would have never made it. I would also like to thank Prof. David Richards, who was the Head of the Physics Department in 2015 and who admitted me to the program. And of course I'd like to thank my MPhil Supervisor Prof. Malcolm Fairbairn for helping me prepare this thesis and my MPhil examiners Dr Christopher McCabe and Dr Alkistis Pourtsidou for taking the time to go through this report and for conducting the oral examination. Finally, I'd like to thank other colleagues in the King's College London Physics department for interesting and insightful discussions and seminars, many of which were to various degrees important for me during my work on this project.

References

[1] D. R. Lorimer, M. Bailes, M. A. McLaughlin, D. J. Narkevic, and F. Crawford, "A Bright Millisecond Radio Burst of Extragalactic Origin," *Science*, vol. 318, p. 777, Nov. 2007.

[2] M. Amiri *et al.*, "Observations of fast radio bursts at frequencies down to 400 megahertz," *Nature*, vol. 566, no. 7743, pp. 230–234, 2019.

[3] D. Thornton, B. Stappers, M. Bailes, B. Barsdell, S. Bates, N. D. R. Bhat, M. Burgay, S. Burke-Spolaor, D. J. Champion, P. Coster, N. D'Amico, A. Jameson, S. Johnston, M. Keith, M. Kramer, L. Levin, S. Milia, C. Ng, A. Possenti, and W. van Straten, "A population of fast radio bursts at cosmological distances," *Science*, vol. 341, no. 6141, pp. 53–56, 2013.

[4] E. F. Keane, B. W. Stappers, M. Kramer, and A. G. Lyne, "On the origin of a highly dispersed coherent radio burst," *Monthly Notices of the Royal Astronomical Society: Letters*, vol. 425, no. 1, pp. L71–L75, 2012.

[5] M. Caleb *et al.*, "The first interferometric detections of Fast Radio Bursts," *Mon. Not. Roy. Astron. Soc.*, vol. 468, no. 3, pp. 3746–3756, 2017.

[6] P. Bull *et al.*, "Fundamental Physics with the Square Kilometer Array," 2018.

[7] T. C. Collaboration, M. Amiri, K. Bandura, P. Berger, M. Bhardwaj, M. M. Boyce, P. J. Boyle, C. Brar, M. Burhanpurkar, P. Chawla, J. Chowdhury, J.-F. Cliche, M. D. Cranmer, D. Cubranic, M. Deng, N. Denman, M. Dobbs, M. Fandino, E. Fonseca, B. M. Gaensler, U. Giri, A. J. Gilbert, D. C. Good, S. Guliani, M. Halpern, G. Hinshaw, C. HÃűfer, A. Josephy, V. M. Kaspi, T. L. Landecker, D. Lang, H. Liao, K. W. Masui, J. Mena-Parra, A. Naidu, L. B. Newburgh, C. Ng, C. Patel, U.-L. Pen, T. Pinsonneault-Marotte, Z. Pleunis, M. R. Ravandi, S. M. Ransom, A. Renard, P. Scholz, K. Sigurdson, S. R. Siegel, K. M. Smith, I. H. Stairs, S. P. Tendulkar, K. Vanderlinde, and D. V. Wiebe, "The chime fast radio burst project: System overview," *The Astrophysical Journal*, vol. 863, no. 1, p. 48, 2018.

[8] A. D. Bolatto, S. Chatterjee, C. M. Casey, L. Chomiuk, I. de Pater, M. Dickinson, J. Di Francesco, G. Hallinan, A. Isella, K. Kohno, S. R. Kulkarni, C. Lang, T. J. W. Lazio, A. K. Leroy, L. Loinard, T. J. Maccarone, B. C. Matthews, R. A. Osten, M. J. Reid, D. Riechers, N. Sakai, F. Walter, and D. Wilner, "Key Science Goals for the Next Generation Very Large Array (ngVLA): Report from the ngVLA Science Advisory Council," *ArXiv e-prints*, Nov. 2017.

[9] M. F. Bietenholz and N. Bartel, "On the Possibility of Fast Radio Bursts from Inside Supernovae: The Case of SN 1986J," *Astrophys. J.*, vol. 851, no. 2, p. 124, 2017.

[10] P. Das Gupta and N. Saini, "Collapsing supra-massive magnetars: FRBs, the repeating FRB121102 and GRBs," in *Journal of Astrophysics and Astronomy, Volume 39, Issue 1, February 2018*, 2017.

[11] M. Lingam and A. Loeb, "Fast radio bursts from extragalactic light sails," *The Astrophysical Journal Letters*, vol. 837, no. 2, p. L23, 2017.

[12] L. G. Spitler *et al.*, "Fast radio burst discovered in the arecibo pulsar alfa survey," *The Astrophysical Journal*, vol. 790, no. 2, p. 101, 2014.

[13] S. Chatterjee *et al.*, "The direct localization of a fast radio burst and its host," *Nature*, vol. 541, p. 58, 2017.

[14] B. D. Metzger, E. Berger, and B. Margalit, "Millisecond Magnetar Birth Connects FRB 121102 to Superluminous Supernovae and Long Duration Gamma-ray Bursts," *Astrophys. J.*, vol. 841, no. 1, p. 14, 2017.

[15] C. G. Bassa *et al.*, "FRB 121102 is coincident with a star forming region in its host galaxy," *Astrophys. J.*, vol. 843, no. 1, p. L8, 2017.

[16] K. Hurley *et al.*, "A Tremendous flare from SGR1806-20 with implications for short-duration gamma-ray bursts," *Nature*, vol. 434, pp. 1098–1103, 2005.

[17] K. W. Bannister, A. T. Deller, C. Phillips, J.-P. Macquart, J. X. Prochaska, N. Tejos, S. D. Ryder, E. M. Sadler, R. M. Shannon, S. Simha, C. K. Day, M. McQuinn, F. O. North-Hickey, S. Bhandari, W. R. Arcus, V. N. Bennert, J. Burchett, M. Bouwhuis, R. Dodson, R. D. Ekers, W. Farah, C. Flynn, C. W. James, M. Kerr, E. Lenc, E. K. Mahony, J. O'Meara, S. Osłowski, H. Qiu, T. Treu, V. U, T. J. Bateman, D. C.-J. Bock, R. J. Bolton, A. Brown, J. D. Bunton, A. P. Chippendale, F. R. Cooray, T. Cornwell, N. Gupta, D. B. Hayman, M. Kesteven, B. S. Koribalski, A. MacLeod, N. M. McClure-Griffiths, S. Neuhold, R. P. Norris, M. A. Pilawa, R.-Y. Qiao, J. Reynolds, D. N. Roxby, T. W. Shimwell, M. A. Voronkov, and C. D. Wilson, "A single fast radio burst localized to a massive galaxy at cosmological distance," *Science*, 2019.

[18] V. Ravi, M. Catha, L. D Addario, S. G. Djorgovski, G. Hallinan, R. Hobbs, J. Kocz, S. R. Kulkarni, J. Shi, H. Vedantham, S. Weinreb, and D. Woody, "A fast radio burst localized to a massive galaxy," *Nature*, 07 2019.

[19] R. H. Dicke, "Coherence in spontaneous radiation processes," *Phys. Rev.*, vol. 93, pp. 99–110, Jan 1954.

[20] W. H. Press and S. A. Teukolsky, "Floating Orbits, Superradiant Scattering and the Black-hole Bomb," *Nature*, vol. 238, pp. 211–212, 1972.

[21] R. Brito, V. Cardoso, and P. Pani, eds., *Superradiance*, vol. 906 of *Lecture Notes in Physics, Berlin Springer Verlag*, 2015.

[22] J. P. Conlon and C. A. R. Herdeiro, "Can black hole superradiance be induced by galactic plasmas?," *Phys. Lett.*, vol. B780, pp. 169–173, 2018.

[23] S. M. C. V. Goncalves, "Black hole formation from massive scalar field collapse in the Einstein-de Sitter universe," *Phys. Rev.*, vol. D62, p. 124006, 2000.

[24] P. A. R. Ade *et al.*, "Planck 2015 results. XIII. Cosmological parameters," *Astron. Astrophys.*, vol. 594, p. A13, 2016.

[25] G. Bertone, D. Hooper, and J. Silk, "Particle dark matter: Evidence, candidates and constraints," *Phys. Rept.*, vol. 405, pp. 279–390, 2005.

[26] D. J. E. Marsh, "Axion Cosmology," *Phys. Rept.*, vol. 643, pp. 1–79, 2016.

[27] A. Boyarsky, M. Drewes, T. Lasserre, S. Mertens, and O. Ruchayskiy, "Sterile Neutrino Dark Matter," 2018.

[28] B. Carr, F. Kühnel, and M. Sandstad, "Primordial black holes as dark matter," *Phys. Rev. D*, vol. 94, p. 083504, Oct 2016.

[29] D. Baumann, "Inflation," in *Physics of the large and the small, TASI 09, proceedings of the Theoretical Advanced Study Institute in Elementary Particle Physics, Boulder, Colorado, USA, 1-26 June 2009*, pp. 523–686, 2011.

[30] V. Afonso, G. J. Olmo, and D. Rubiera-Garcia, "Scalar geons in born-infeld gravity," *Journal of Cosmology and Astroparticle Physics*, vol. 2017, no. 08, p. 031, 2017.

[31] V. Domcke, F. Muia, M. Pieroni, and L. T. Witkowski, "Pbh dark matter from axion inflation," *Journal of Cosmology and Astroparticle Physics*, vol. 2017, no. 07, p. 048, 2017.

[32] B. P. Abbott *et al.*, "Observation of gravitational waves from a binary black hole merger," *Phys. Rev. Lett.*, vol. 116, p. 061102, Feb 2016.

[33] S. Bird, I. Cholis, J. B. Munoz, Y. Ali-HaÃŕmoud, M. Kamionkowski, E. D. Kovetz, A. Raccanelli, and A. G. Riess, "Did LIGO detect dark matter?," *Phys. Rev. Lett.*, vol. 116, no. 20, p. 201301, 2016.

[34] S. Clesse and J. Garcia-Bellido, "Seven hints for primordial black hole dark matter," *Physics of the Dark Universe*, vol. 22, 11 2017.

[35] P. Pani and A. Loeb, "Constraining primordial black-hole bombs through spectral distortions of the cosmic microwave background," *Phys. Rev. D*, vol. 88, p. 041301, Aug 2013.

[36] S. Clesse and J. Garcia-Bellido, "Massive Primordial Black Holes from Hybrid Inflation as Dark Matter and the seeds of Galaxies," *Phys. Rev.*, vol. D92, no. 2, p. 023524, 2015.

[37] A. Fialkov and A. Loeb, "A Fast Radio Burst Occurs Every Second throughout the Observable Universe," *Astrophys. J.*, vol. 846, no. 2, p. L27, 2017.

[38] J. I. Katz, "Fast radio bursts - A brief review: Some questions, fewer answers," *Mod. Phys. Lett.*, vol. A31, no. 14, p. 1630013, 2016.

[39] F. Crawford, A. Rane, L. Tran, K. Rolph, D. R. Lorimer, and J. P. Ridley, "A Search for Highly Dispersed Fast Radio Bursts in Three Parkes Multibeam Surveys," *Mon. Not. Roy. Astron. Soc.*, vol. 460, no. 3, pp. 3370–3375, 2016.

[40] H. Ratcliffe, *Electron Beam Evolution and Radio Emission in the Inhomogeneous Solar Corona*. PhD thesis, 2013.

[41] M. Visser, "The Kerr spacetime: A Brief introduction," in *Kerr Fest: Black Holes in Astrophysics, General Relativity and Quantum Gravity Christchurch, New Zealand, August 26-28, 2004*, 2007.

[42] D. Huterer and D. L. Shafer, "Dark energy two decades after: Observables, probes, consistency tests," *Rept. Prog. Phys.*, vol. 81, no. 1, p. 016901, 2018.

[43] K. Freese, "Status of Dark Matter in the Universe," *Int. J. Mod. Phys.*, vol. 1, no. 06, pp. 325–355, 2017.

[44] G. Tormen, F. R. Bouchet, and S. D. M. White, "The Structure and dynamical evolution of dark matter halos," *Mon. Not. Roy. Astron. Soc.*, vol. 286, pp. 865–884, 1997.

[45] J. F. Navarro, C. S. Frenk, and S. D. M. White, "The Structure of cold dark matter halos," *Astrophys. J.*, vol. 462, pp. 563–575, 1996.

[46] E. Romano-Diaz, Y. Hoffman, C. Heller, A. Faltenbacher, D. Jones, and I. Shlosman, "Evolution of characteristic quantities for dark matter halo density profiles," *The Astrophysical Journal*, vol. 657, no. 1, p. 56, 2007.

[47] A. Klypin, G. Yepes, S. Gottlober, F. Prada, and S. Hess, "Multidark simulations: the story of dark matter halo concentrations and density profiles," *Monthly Notices of the Royal Astronomical Society*, vol. 457, no. 4, pp. 4340–4359, 2016.

[48] C. C. Onuchukwu and A. C. Ezeribe, "Constraining The Hubble Parameter Using Distance Modulus - Redshift Relation," *ArXiv e-prints*, July 2015.

[49] I. Ferrero, M. G. Abadi, J. F. Navarro, L. V. Sales, and S. Gurovich, "The dark matter haloes of dwarf galaxies: a challenge for the lambda cold dark matter paradigm?," *Monthly Notices of the Royal Astronomical Society*, vol. 425, no. 4, pp. 2817–2823, 2012.

[50] Q. Guo, S. White, C. Li, and M. Boylan-Kolchin, "How do galaxies populate Dark Matter halos?," *Mon. Not. Roy. Astron. Soc.*, vol. 404, p. 1111, 2010.

[51] R. Yan, K. Bundy, D. R. Law, M. A. Bershady, B. Andrews, B. Cherinka, A. M. Diamond-Stanic, N. Drory, N. MacDonald, J. R. Sanchez-Gallego, D. Thomas, D. A. Wake, A.-M. Weijmans, K. B. Westfall, K. Zhang, A. Aragon-Salamanca, F. Belfiore, D. Bizyaev, G. A. Blanc, M. R. Blanton, J. Brownstein, M. Cappellari, R. D'Souza, E. Emsellem, H. Fu, P. Gaulme, M. T. Graham, D. Goddard, J. E. Gunn, P. Harding, A. Jones, K. Kinemuchi, C. Li, H. Li, R. Maiolino, S. Mao, C. Maraston, K. Masters, M. R. Merrifield, D. Oravetz, K. Pan, J. K. Parejko, S. F. Sanchez, D. Schlegel, A. Simmons, K. Thanjavur, J. Tinker, C. Tremonti, R. van den Bosch, and Z. Zheng, "Sdss-iv manga ifs galaxy survey-survey design, execution, and initial data quality," *The Astronomical Journal*, vol. 152, no. 6, p. 197, 2016.

[52] M. Boylan-Kolchin, J. S. Bullock, and M. Kaplinghat, "Too big to fail? the puzzling darkness of massive milky way subhaloes," *Monthly Notices of the Royal Astronomical Society: Letters*, vol. 415, no. 1, pp. L40–L44, 2011.

[53] Q. Guo, S. White, M. Boylan-Kolchin, G. D. Lucia, G. Kauffmann, G. Lemson, C. Li, V. Springel, and S. Weinmann, "From dwarf spheroidals to cd galaxies: simulating the galaxy population in a lcdm cosmology," *Monthly Notices of the Royal Astronomical Society*, vol. 413, no. 1, pp. 101–131.

[54] H. C. Plummer, "On the problem of distribution in globular star clusters," *Mon. Not. Roy. Astron. Soc.*, vol. 71, pp. 460–470, 1911.

[55] T. Ichikawa, M. Kajisawa, and M. Akhlaghi, "A universal stellar mass-size relation of galaxies in the goods-north region," *Monthly Notices of the Royal Astronomical Society*, vol. 422, no. 2, pp. 1014–1027, 2012.

[56] G. J. Mathews, M. Kusakabe, and T. Kajino, "Introduction to Big Bang Nucleosynthesis and Modern Cosmology," *Int. J. Mod. Phys.*, vol. E26, no. 08, p. 1741001, 2017.

[57] C. J. Conselice, "The Evolution of Galaxy Structure over Cosmic Time," *Ann. Rev. Astron. Astrophys.*, vol. 52, pp. 291–337, 2014.

[58] M. Kajisawa, T. Ichikawa, I. Tanaka, T. Yamada, M. Akiyama, R. Suzuki, C. Tokoku, Y. K. Uchimoto, M. Konishi, T. Yoshikawa, T. Nishimura, K. Omata, M. Ouchi, I. Iwata, T. Hamana, and M. Onodera, "Moircs deep survey. ix. deep near-infrared imaging data and source catalog," *Publications of the Astronomical Society of Japan*, vol. 63, no. sp2, pp. S379–S401, 2011.

[59] B. W. Holwerda, *Source extractor for dummies v5*. PhD thesis, Baltimore, Space Telescope Sci., 2005.

[60] M. Kajisawa, T. Ichikawa, I. Tanaka, M. Konishi, T. Yamada, M. Akiyama, R. Suzuki, C. Tokoku, Y. K. Uchimoto, T. Yoshikawa, M. Ouchi, I. Iwata, T. Hamana, and M. Onodera, "Moircs deep survey. iv. evolution of galaxy stellar mass function back to z=3," *The Astrophysical Journal*, vol. 702, no. 2, p. 1393, 2009.

[61] T. C. Licquia and J. A. Newman, "Improved estimates of the milky way's stellar mass and star formation rate from hierarchical bayesian meta-analysis," *The Astrophysical Journal*, vol. 806, no. 1, p. 96, 2015.

[62] D. J. E. Marsh and J. Silk, "A Model For Halo Formation With Axion Mixed Dark Matter," *Mon. Not. Roy. Astron. Soc.*, vol. 437, no. 3, pp. 2652–2663, 2014.

[63] F. Crawford, A. Rane, L. Tran, K. Rolph, D. R. Lorimer, and J. P. Ridley, "A search for highly dispersed fast radio bursts in three parkes multibeam surveys," *Monthly Notices of the Royal Astronomical Society*, vol. 460, no. 3, pp. 3370–3375, 2016.

[64] S. M. Koushiappas and A. Loeb, "Dynamics of Dwarf Galaxies Disfavor Stellar-Mass Black Holes as Dark Matter," *Phys. Rev. Lett.*, vol. 119, no. 4, p. 041102, 2017.

[65] B. Carr and J. Silk, "Primordial Black Holes as Generators of Cosmic Structures," *Mon. Not. Roy. Astron. Soc.*, vol. 478, no. 3, pp. 3756–3775, 2018.

[66] D. J. Bacon *et al.*, "Cosmology with Phase 1 of the Square Kilometre Array: Red Book 2018: Technical specifications and performance forecasts," *Submitted to: Publ. Astron. Soc. Austral.*, 2018.

[67] D. Li and Z. Pan, "The Five-hundred-meter Aperture Spherical Radio Telescope Project," *Radio Science*, vol. 51, pp. 1060–1064, July 2016.